Engineered Science

RESEARCH PAPER

View Article Online

Chitosan-coated-magnetite with Covalently Grafted Polystyrene Based Carbon Nanocomposites for Hexavalent Chromium Adsorption

Hongbo Gu,*[1] Xiaojiang Xu,[1] Hongyuan Zhang,[1] Chaobo Liang,[3] Han Lou,[1] Chao Ma,[1] Yujie Li,[1] Zhanhu Guo[2] and Junwei Gu*[3]

A chitosan-coated-magnetite with covalently grafted polystyrene (*g*-PS) based magnetic carbon nanocomposites composed of carbon coated magnetite nanoparticles with carbonized *g*-PS microsphere are prepared for effective hexavalent chromium (Cr(VI)) adsorption. The adsorption measurements have indicated that the fabricated magnetic nanocomposites FC515 exhibit an effective Cr(VI) adsorption performance and the optimal pH for Cr(VI) adsorption on FC515 is 3.0 at 298 K. The Cr(VI) adsorption kinetics on FC515 is found to follow the pseudo-second-order behavior with a room temperature initial adsorption rate of 7.106 g mg^{-1} min^{-1} for the solution with an initial Cr(VI) concentration of 6.5 mg L^{-1} and pH value of 3.0. The adsorption isotherm test illustrates that the Langmuir isotherm model with a monolayer adsorption is well fitted for Cr(VI) adsorption on FC515 than the Freundlich isotherm model. The thermodynamic parameters including negative standard Gibb's free energy change and standard enthalpy change suggest that the Cr(VI) adsorption on FC515 is spontaneous and exothermic. After 5 cycles, FC515 still maintain 86% of Cr(VI) adsorption capacity, exhibiting a good reusability in practice. The zeta-potential and X-ray photoelectron spectroscopy (XPS) measurements demonstrate that the Cr(VI) adsorption on FC515 is mainly from the electrostatic interaction between FC515 and Cr(VI). This work provides a new method to design the novel structure of magnetic carbon nanocomposites with natural polymer chitosan and thermoplastic PS for Cr(VI) wastewater treatment.

Keywords: Chitosan; Magnetite; Grafted polystyrene; Carbon nanocomposites; Cr(VI) adsorption

Received 11th February 2018, Accepted 4th March 2018

DOI: 10.30919/espub.es.180308

1. Introduction

Hexavalent chromium (Cr(VI)) released from electroplating, leather tanning, printing, and pigments is considered as a hazardous and toxic contaminant in water system.[1] In order to achieve the US Environmental Protection Agency (US-EPA) limitation (total Cr lower than 100 μg L^{-1} in drinking water),[2,3] it's urgently required to remove Cr(VI) from waste water system. Currently, among various kinds of technologies for Cr(VI) removal from wastewater including chemical precipitation, ion exchange, membrane filtration, and biomass, adsorption is a competitive method due to its simplicity, low cost, and high efficiency.[4] Hence, it's demanded to design and develop the novel adsorbent materials towards Cr(VI) removal with high efficiency and low cost.

Chitosan is an abundant natural aminopolysaccharide containing both of glucosamine and acetylglucosamine moieties, which is derived from the N-deacetylation of chitin.[5] The amino and hydroxyl groups on the polymer backbone of chitosan are able to serve as the chelating sites for the removal of heavy metals from polluted water.[6] However, the adsorption performance of chitosan is normally controlled by the molecular weight and deacetylation degree of the raw chitin.[7] In addition, chitosan is sensitive to the solution pH. On the one hand, it's easily dissolved in the acidic solution (especially as solution pH is less than 5); on the other hand, the protonation of amino group on chitosan in the acidic solution could severely decrease its adsorption capacity.[8] Therefore, it's commonly needed to be crosslinked to enhance the stability of chitosan. Laus *et al.*[9] used epichorohydrin (ECH) and triphosphate (TPP) to covalently crosslink with chitosan as the adsorbent, which possessed the maximum adsorption capacities for Cu(II), Cd(II), and Pb(II) of 130.72, 83.75, and 166.94 mg g^{-1}, respectively. Wu *et al.*[10] utilized ECH and triethylenetetramine (TETA) to graft and crosslink chitosan and the obtained modified chitosan exhibited adsorption capacity for Cu(II) and Ag(I) of 117.6 and 151.20 mg L^{-1}, respectively. Also, chitosan often serves as the shell material to prepare the magnetic chitosan nanocomposites for heavy metal removal in order to easy recycle and reuse the adsorbents. Chen *et al.*[11] prepared the magnetic nanosized

[1] *Shanghai Key Lab of Chemical Assessment and Sustainability, Department of Chemistry, Tongji University, Shanghai 200092, People's Republic of China. E-mail: hongbogu2014@tongji.edu.cn*

[2] *Integrated Composites Laboratory (ICL), Department of Chemical & Biomolecular Engineering, University of Tennessee, Knoxville, Tennessee, 37966, USA*

[3] *MOE Key Laboratory of Material Physics and Chemistry under Extraordinary Conditions, Shaanxi Key Laboratory of Macromolecular Science and Technology, Department of Applied Chemistry, School of Science, Northwestern Polytechnical University, Xi' an, Shaanxi, 710072, P. R. China. E-mail: gjw@nwpu.edu.cn*

chitosan composites, which exhibited the maximum Cu(II) adsorption capacity of 35.5 mg g^{-1}. Zhu *et al.*[12] studied the adsorption properties of Pb(II), Cu(II), Zn(II) onto xanthate-modified magnetic chitosan and the maximum adsorption capacities for Pb(II), Cu(II), Zn(II) were 76.9, 34.5, and 20.8 mg g^{-1}, respectively. Yet, even the magnetic chitosan could be manipulated by an external magnetic field, the coating material chitosan still has the poor acid resistant property. The crosslinking process may also reduce the adsorption capability of chitosan, especially if this process involves in the reaction of amino groups.[13]

In recent years, magnetic carbon nanocomposites have gained considerable attentions in the heavy metal adsorption due to the high specific surface area and good environmental stability of carbon materials, and easy recycle process of magnetic materials. The carbon shell could protect the magnetic metal oxides from the acid etching and the magnetic core could help recycle of nanocomposites and reuse it for the heavy metal removal. Therefore, many efforts have been dedicated to the preparation of magnetic carbon nanocomposites with novel structures. However, there is still no report on the chitosan based magnetic carbon nanocomposites. Currently, in our previous work, the ECH grafted polystyrene (PS) has served as the carbon precursor to form the magnetic carbon nanocomposites for organic pollutant tetrabromobisphenol A (TBBPA)[14] and toxic heavy metal Cr(VI) removal.[2] Nevertheless, both PS and chitosan behaved as the carbon precursor to prepare the magnetic carbon nanocomposites for heavy metal removal are rarely reported.

In this paper, magnetite nanoparticles were prepared by a co-precipitation method with the *n*-octanoic acid as a surfactant, and the chitosan-coated-magnetite with covalently grafted polystyrene based magnetic carbon nanocomposites were synthesized by the chemical reaction combined with high temperature annealing. The effects of parameters during high temperature annealing process on the specific surface area, microstructure and adsorption effect of magnetic carbon nanocomposites were studied. The microstructure, crystal structure, thermal oxidation degradation performance, and magnetic properties of magnetic carbon nanocomposites were determined by a series of characterizations including scanning electron microscope (SEM), transmission electron microscopy (TEM), X-ray diffraction (XRD), and thermogravimetric analysis (TGA). The recovery and reuse performance of magnetic carbon nanocomposites were evaluated by the cyclic adsorption experiments. The Cr(VI) adsorption characteristics was analyzed by adsorption kinetics, isothermal adsorption and adsorption thermodynamics. Finally, zeta potential and XPS characterization were used to explore the Cr(VI) adsorption mechanism. This work is aiming to design a novel magnetic carbon nanocomposite structures with chitosan and PS for Cr(VI) removal from wastewater system.[15]

2. Experiment

2.1. Materials

Aluminum chloride anhydrous ($AlCl_3$), ferric chloride (hexahydrate) ($FeCl_3{\cdot}6H_2O$), ethyl acetate ($C_4H_8O_2$), ferrous sulfate (heptahydrate) ($FeSO_4{\cdot}7H_2O$), chitosan($(C_6H_{11}NO_4)_n$), ethanol (95%, v/v), anhydrous ethanol, acetone (C_3H_6O), epichlorohydrin (C_3H_5ClO), cyclohexane (C_6H_{12}) and ammonium hydroxide ($NH_3{\cdot}H_2O$, 25~28 wt%) were supplied by Sinopharm Chemical Reagent Co., Ltd. Polystyrene (PS) was purchased from Taizhou Suosi education equipment Co., Ltd. 1-butyl-3-methylimidazole ($C_8H_{15}ClN_2$) and *n*-octanoic acid ($C_8H_{12}O_2$) was provided from TCI Company, Shanghai. All the chemicals were used as-received without any further treatment.

2.2. Fabrication of chitosan-coated-magnetite with covalently grafted PS based carbon nanocomposites

First, the PS was grafted with epichlorohydrin (*g*-PS) as published in the previous work.[16] Second, the $FeSO_4{\cdot}7H_2O$ and $FeCl_3{\cdot}6H_2O$ with a mole ratio of 1:2 were dissolved in deionized water (25 mL) at room temperature under the magnetic stirring. After that, *n*-octanoic acid (1.0 mL) was dripped in the above solution and the ammonium hydroxide was added until pH to 10-11. The solution was kept at 80 °C in a water bath for 1 h to form the magnetite nanoparticles. Then, the mixture was respectively washed with deionized water and 95% (v/v) ethanol for three times, and dried in an oven at 60 °C for 6 h. The sample was calcined in a tube furnace at 350 °C for 2 h in N_2 atmosphere in order to increase the crystallinity of magnetite nanoparticles. Third, the magnetite (0.25 g), chitosan (0.25 g) and 1-butyl-3-methylimidazolium (ionic liquid, 7.0 g) were put in a 25 mL of beaker, and the mixture was heated to 50 °C in a water bath and mechanically stirred for 1 h. Then, the mixture was washed with deionized water to completely remove the ionic liquid. The mixture was filtered and washed with deionized water and 95% (v/v) ethanol, separately, for three times, and then dried in an oven at 60 °C for 12 h. Finally, the *g*-PS solution was transferred into a 50 mL of three-necked flask, and 0.5 g of chitosan-coated-magnetite nanocomposites was ultrasonically added into the above solution and reflux at 80 °C for 1 h. The mixed solution was washed with ethanol for five times, and dried in an oven at 60 °C for 12 h. The FTIR and TGA shown in Figure S1 affirms the formation of covalent bond between chitosan coated magnetite and *g*-PS. Then the dried samples were placed in a tube furnace and calcined under the N_2 atmosphere to obtain the magnetic carbon nanocomposites. The preparation procedure of chitosan-coated-magnetite with covalently grafted PS based carbon nanocomposites is displayed in Scheme 1. The samples prepared at 450 °C with calcination time of 30 min; 500 °C with calcination time of 0, 15, and 30 min; 600 °C with calcination time of 30 min were respectively indexed as FC430, FC500, FC515, FC530 and FC630. For details, please see supporting information.

2.3. Characterizations

SEM (S-4800 high-resolution field emission scanning electron microscope) and TEM (Tecnai G20 type transmission electron microscopy) were used to observe the microstructures of samples. The thermal oxidation degradation characteristics of the samples were investigated by a STA 409 differential scanning calorimeter. The TGA curve was recorded at a heating rate of 20 °C min^{-1} within a temperature range from 25 to 850 °C and an air flow rate of 20 mL min^{-1}. The crystalline structure of samples was characterized by a D8 Advance X-ray powder diffractometer with Cu-Kα as the diffractive light source (λ = 1.5406 Å) within the diffraction angle ranges from 10 to 70 ° at a scanning speed of 10 ° min^{-1}. The element composition and valence state of the prepared samples were analyzed by an AXIS Ultra DLD

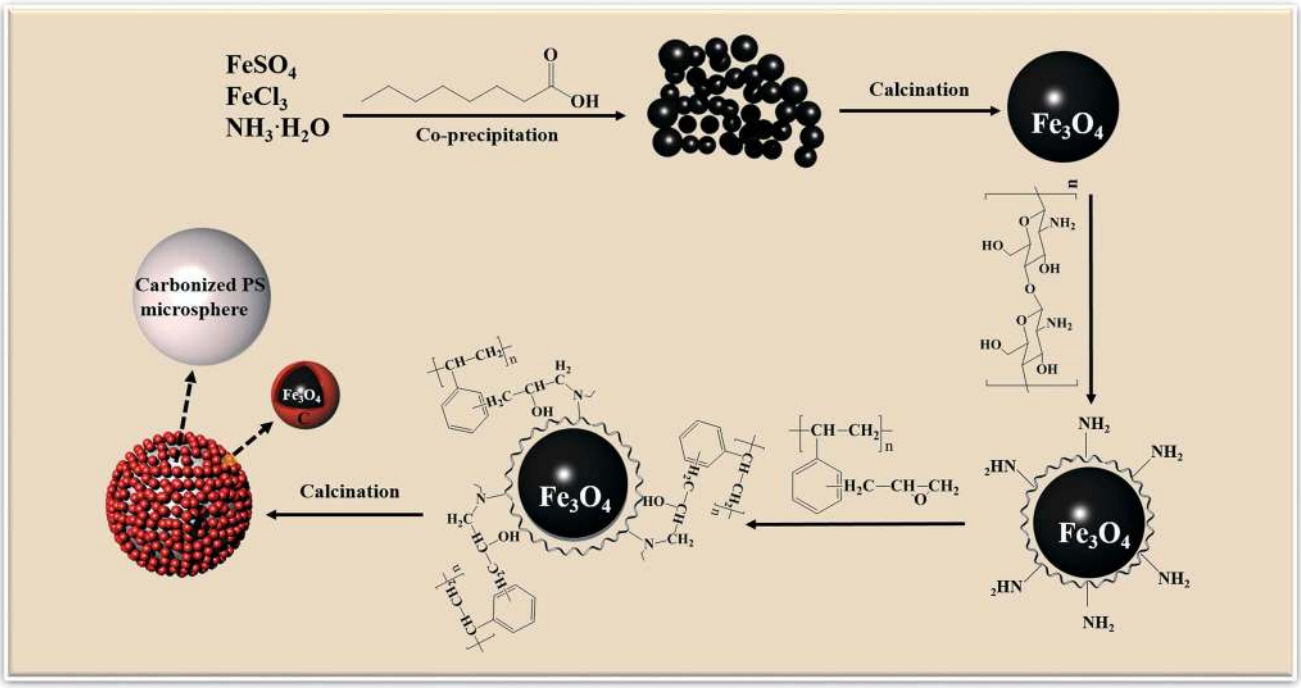

Scheme 1 Schematic for the preparation process of chitosan-coated-magnetite with covalently grafted PS based magnetic carbon nanocomposites.

X-ray photoelectron spectroscopy (XPS). The radiation source was Al-Kα (hυ = 1486.6 eV) with an operating voltage of 12 kV and a current of 10 mA, respectively. The resulting element was deconvoluted into peaks on a Shirley background using the Gaussian-Lorentz function (Gaussian = 80%, Lorentzian = 20%). The specific surface area and pore size distribution of the samples were conducted by a Tristar 3020 specific surface area and porosity analyzer. The specific surface area and pore size distribution of samples were calculated based on the BET (Brunauer-Emmett-Teller) equation and the BJH (Barrett-Joyner-Halenda) model. Magnetic measurement was performed on a PPMS-9T (EC-II) physical measurement system at a temperature of 298 K within the magnetic field range of 0-3 T. The surface zeta potentials of the nanoadsorbents were determined by a DLS Particle Size analyzer (Zetasizer Nano-ZS, Malvern, U.K.).

2.4. Cr(VI) adsorption measurements

Cr(VI) adsorption characteristics by the as-prepared magnetic carbon nanoadsorbents was evaluated and all the measurements were conducted in a thermostatic ultrasonic cleaner (model: KH5200DE). The concentration of Cr(VI) was determined by an inductively coupled plasma optical emission spectrometry (ICP-OES, 8300). The initial Cr(VI) concentration was adjusted by diluting 1.0 g L^{-1} of stock solution with deionized water. The reported value for each sample was the average of three measurements with a standard deviation of ±5%. The Cr(VI) adsorption amounts q_t and the Cr(VI) removal percentage (R%) were respectively calculated through Equation (S1) and (S2). The details for Cr(VI) adsorption experiments please refer to supporting information.

3. Results and discussion

3.1. Optimal preparation conditions exploration of magnetic carbon nanocomposites

In order to study the optimal preparation conditions of magnetic carbon nanocomposites, the BET specific surface area of magnetic carbon nanocomposites prepared under different conditions including FC430, FC500, FC515, FC530, and FC630 is analyzed since the BET results are related to the adsorption performance of materials and the results are shown in Table S1. The FC430, FC500, FC530 and FC630 have a specific surface area of 25, 41, 30, and 24 m^2 g^{-1}, accordingly. And the magnetic nanocomposite FC515 calcined at 500 ^oC for 15 min possesses the largest specific surface area of 58 m^2 g^{-1}. This illustrates that different preparation conditions can cause different specific surface areas of magnetic carbon nanocomposites.

Meanwhile, the Cr(VI) removal percentage by these magnetic carbon nanocomposites prepared under different conditions has served as a justification to explore the optimal fabrication conditions of chitosan-coated-magnetite with covalently *g*-PS based magnetic carbon nanocomposites. As mentioned in the experimental section, FC430, FC500, FC515, FC530, and FC630 (10 mg) were added into a 2.0 mg L^{-1} of Cr (VI) solution with a pH of 7.0 for ultrasonic treatment of 5 min and the obtained experimental results are displayed in Figure S2. The removal percentage of Cr(VI) by FC430, FC500, FC515, FC530 and FC630 is 38.6, 59.4, 70.4, 57.0 and 46.4%, respectively. It's concluded that FC515 exhibits the highest Cr (VI) removal percentage.

Based on the BET results and Cr(VI) removal performance, the optimum conditions for the preparation of magnetic carbon nanocomposites are at a temperature of 500 ^oC for 15 min in the N_2

atmosphere (FC515). The subsequent experiments were conducted by using FC515.

3.2. Structure characterization of FC515

In order to study the microstructure characteristics of samples, the SEM images with high and low magnifications for as-prepared Fe_3O_4, chitosan coated Fe_3O_4 and FC515 have been performed and the obtained results are depicted in Figure S3. The SEM images of Fe_3O_4 with and without *n*-octanoic acid are shown in Figure S4. The results manifest that after adding *n*-octanoic acid, the morphology of Fe_3O_4 nanoparticles becomes uniform. This confirms the role of *n*-octanoic acid as a surfactant. In Figure S3a and d, it's seen that the as-prepared Fe_3O_4 has a spherical structure with a smooth surface and an average diameter about 20-30 nm. After coated with chitosan, Figure S3b and e, the surface of Fe_3O_4 become relatively rougher. However, the FC515 has a totally different microstructure, which is composed of big carbon microspheres surrounded by small nanoparticles, Figure S3c and f. The big carbon microsphere probably from the functionalized PS has a diameter of 300-400 nm. The small nanoparticles may be caused by the carbonized chitosan coated Fe_3O_4.

In the TEM images, Figure 1a, it's observed that the average diameter of Fe_3O_4 is about 20-30 nm, which is consistent with SEM results, Figure S3a. After coated with Fe_3O_4, Figure 1b, there is an obvious chitosan polymer layer on the surface of Fe_3O_4 nanoparticles. In the TEM image of FC515, Figure 1d, it's seen that FC515 consists of a big amorphous carbon sphere with a lot of small nanoparticles around. After magnifying the small nanoparticles to the high resolution TEM, Figure 1c, it's found that these small nanoparticles possess a core-shell structure comprised of a crystalline structure and an amorphous carbon layer. In the crystalline structure, the lattice distance is calculated to be 0.252 nm, corresponding to the (3 1 1) crystallographic planes of Fe_3O_4 (PDF#65-3107).[17] This demonstrates that the small nanoparticles are formed from the carbonized chitosan coated Fe_3O_4, which means that the big amorphous carbon sphere is created by the *g*-PS during the high temperature annealing process. The constructed core-shell nanostructure of calcined chitosan coated Fe_3O_4 can enhance the stability and acid corrosion resistance of Fe_3O_4. These results are in accord with those observed by SEM, Figure S3c.

Figure 2A reveals the wide-angle XRD profiles of Fe_3O_4, chitosan coated Fe_3O_4 and FC515. The diffraction peaks of Fe_3O_4 (Figure 2A-a), chitosan coated Fe_3O_4 (Figure 2A-b) and FC515 (Figure 2A-c) are measured to be around 30.1, 35.5, 43.2, 53.5, 56.9, and 62.6°, which correspond to the (2 0 0), (3 1 1), (4 0 0), (4 2 2), (5 1 1), (4 4 0) crystallographic planes of the spinel phase in Fe_3O_4 (PDF#65-3107), respectively. Obviously, in the chitosan coated Fe_3O_4, the carbon coating does not cause the crystalline phase changes in Fe_3O_4 nanoparticles. According to Scherrer Equation (S3),[18] the reflecting peak at $2\theta = 35.5^{o}$ is selected to calculate the crystallite size of as-prepared products, the average crystallite size of the Fe_3O_4, chitosan coated Fe_3O_4 and FC515 is estimated to be about 17.9, 18.1 and 24.3 nm, respectively, which are consistent with the results obtained from TEM images.[19,20]

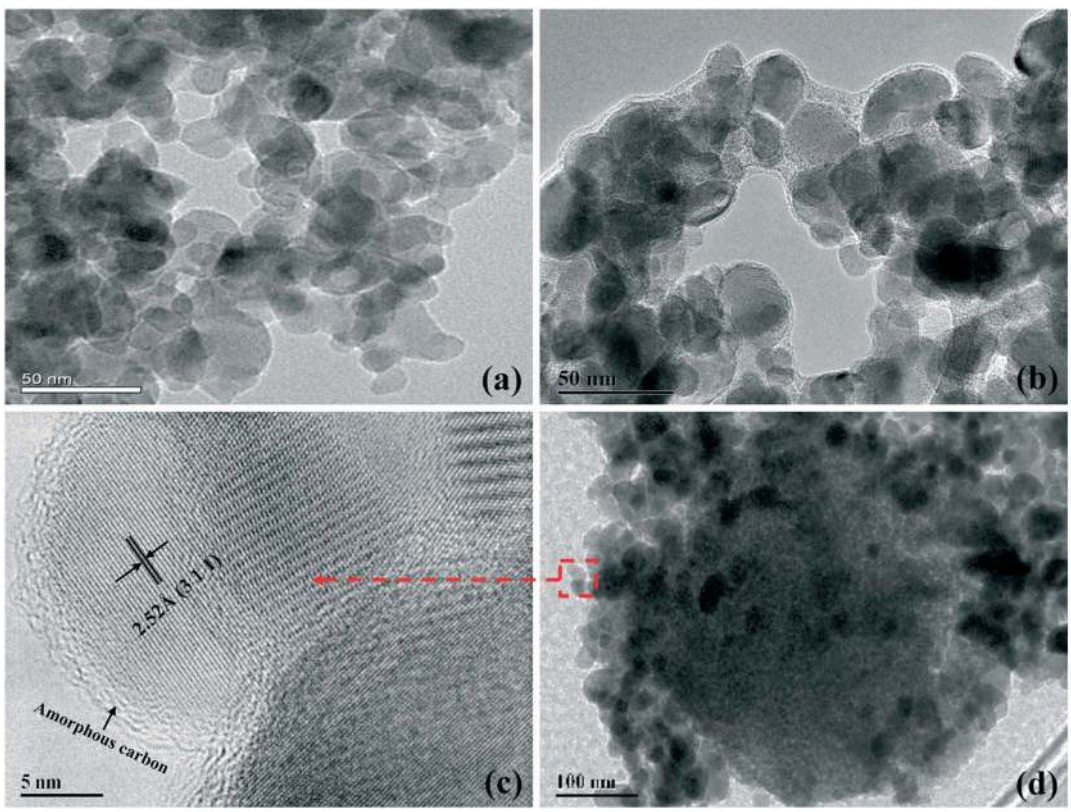

Fig. 1 TEM images of (a) Fe_3O_4, (b) chitosan coated Fe_3O_4, (c) FC515, and (d) HRTEM of small nanoparticles for FC515.

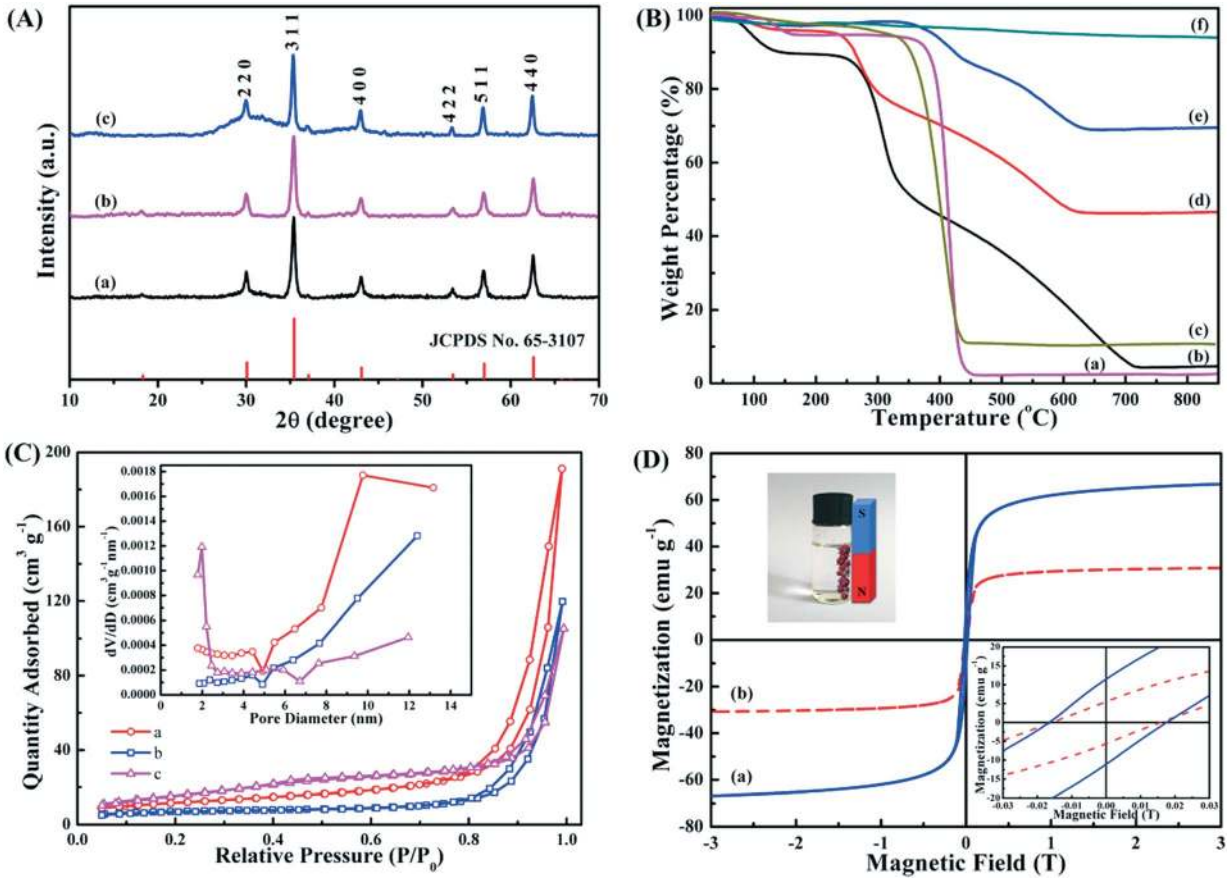

Fig. 2 (A) XRD patterns of (a) Fe_3O_4, (b) chitosan coated Fe_3O_4, (c) FC515; (B) TGA curves of (a) PS, (b) chitosan, (c) *g*-PS, (d) chitosan coated Fe_3O_4, (e) FC515, and (f) Fe_3O_4; (C) nitrogen adsorption-desorption isotherms and pore size distributions of (a) Fe_3O_4, (b) chitosan coated Fe_3O_4, (c) FC515; (D) room temperature magnetization curves of (a) Fe_3O_4, and (b) FC515.

The TGA curves, Figure 2B, illustrate the weight loss of PS, *g*-PS, Fe_3O_4, chitosan, chitosan coated Fe_3O_4 and FC515 within the temperature range from room temperature to 850 °C in the air atmosphere. The result shows that the weight of all the samples is slightly less than 100% before 150 °C, which is attributed to the loss of moisture in the samples. The major weight loss of PS and *g*-PS is from 390 to 450 °C and 300 to 430 °C, Figure 2B-a and c respectively, which is due to the large scale thermal degradation of PS chains. The weight of Fe_3O_4 nanoparticles has no obvious change within the measured temperature range, Figure 2B-f. The decomposition temperature range for chitosan is from 250 to 720 °C, Figure 2B-b, whereas for chitosan coated Fe_3O_4 is from 240 to 620 °C, Figure 2B-d. The percentage of final residue for chitosan coated Fe_3O_4 is 46.6%, indicating that the mass fraction of Fe_3O_4 in chitosan coated Fe_3O_4 is about 46.6%. The thermal degradation temperature of FC515 is divided into two stages, Figure 2B-e, the first stage appears at 350-450 °C, and the second stage is at 450-640 °C. Compared with the degradation temperature of PS, *g*-PS and chitosan, the thermal degradation of the first stage for FC515 mainly arises from the thermal degradation of carbon microspheres formed by carbonization of *g*-PS in FC515, and the second stage in FC515 is from the thermal degradation of carbon layer formed by chitosan. After thermal degradation process, the final residue of FC515 is about 69.5%.

The specific surface area and pore size distribution of the synthesized magnetic carbon nanocomposites are obtained by the nitrogen adsorption and desorption isotherms, Figure 2C. The type-IV adsorption-desorption isotherm curves with the hysteresis loop indicate the mesoporous properties of Fe_3O_4, chitosan coated Fe_3O_4 and FC515.[21] The desorption isotherm is located above the adsorption isotherm with an obvious adsorption hysteresis. Especially, at the higher P/P_0, a typical H3-type hysteresis loop is formed. The obtained BET specific surface area of Fe_3O_4, chitosan coated Fe_3O_4 and FC515 are calculated to be 41, 24 and 58 $m^2\ g^{-1}$, respectively. The pore diameter of Fe_3O_4, chitosan coated Fe_3O_4 and FC515 are in the range of 1-14 nm. It's seen that the there is no obvious peak in the whole pore size distribution range, indicating that they have a wide range of pore size distribution and non-uniform porosity.[22]

Figure 2D displays the magnetization curves of Fe_3O_4 and FC515 at room temperature. Evidently, the magnetization of as-prepared Fe_3O_4 nanoparticles does not reach the saturation state under the magnetic field of ± 3 T, the saturation magnetization (M_s) is intercepted by $M \sim H^{-1}$ (M and H respectively represent the magnetization and magnetic field). The calculated M_s of Fe_3O_4 nanoparticles is 70 emu g^{-1}, which is less than the M_s (about 92 emu g^{-1}) of Fe_3O_4 bulk material.[23] The M_s of FC515 is 31 emu g^{-1}, which is sufficient for the recycling of FC515 as demonstrated on the left top of inset Figure 2D.

3.3. Cr(VI) adsorption evaluation by FC515

Figure 3a shows the Cr(VI) adsorption capacity (q_t) on the FC515 for different treatment time at 298 K and pH of 3.0, which is calculated from Equation (S1). It's observed that the q_t increases fast from 0 to 10 min and then gradually changes from 10 to 30 min. As the treatment time increases further, the q_t is slightly altered. This means that the treatment time for Cr(VI) adsorption on FC515 to reach equilibrium is approximately 30 min. The kinetics for Cr(VI) adsorption on the FC515 is investigated based on the q_t variations with the treatment time. Both the pseudo-first-order and pseudo-second-order adsorption kinetic models are used to express the Cr(VI) adsorption on FC515 as indicated in Equation (S4) and (S5).[24] After fitting, the obtained values of k_1, k_2, q_e, intial adsorption rate (h), and correlation coefficient (r^2) are listed in Table S2. Markedly, the Cr(VI) adsorption kinetics on FC515 is well fitted by the pseudo-second-order model because of the high fitting r^2 (0.974) relative to the pseudo-first-order (r^2 = 0.787). This illustrates that the Cr(VI) adsorption kinetics on FC515 obeys typical pseudo-second-order adsorption kinetics. The initial adsorption rate h is calculated to be 7.106 mg g^{-1} min^{-1}, which is higher than that of magnetic graphene materials (0.28 mg g^{-1} min^{-1}),[25] magnetic polypropylene nanocomposites (0.229 mg g^{-1} min^{-1}),[26] and polyaniline/humic acid (PANI/HA) composites (5.31 mg g^{-1} min^{-1}).[27]

The adsorption isotherm is important for determining the adsorption behavior of an adsorbent.[28] The Cr(VI) adsorption isotherms by FC515 was studied at pH of 3.0. Since the equilibrium time for Cr(VI) on FC515 is approximately 30 min as aforementioned, the treatment time was set to 30 min for the adsorption isotherm experiments to make sure that the equilibrium was achieved. The maximum Cr(VI) adsorption amounts on FC515 within the Cr(VI) concentration range from 1.0 to 10.0 mg L^{-1} are shown in Figure 3b. The obtained equilibrium data are respectively fitted by the Langmuir and the Freundlich models in Equation (S7) and (S8).[29] The obtained fitting parameters for the Langmuir and the Freundlich models are presented in Table S3. The results indicate that the correlation coefficient r^2 of Langmuir model (0.993, 0.991, and 0.991 for 298, 308, and 318 K, respectively) for Cr(VI) adsorption on FC515 is higher than that of Freundlich model (0.969, 0.979, and 0.963 for 298, 308, and 318 K, respectively), indicating that the Cr(VI) adsorption on FC515 can be described as a monolayer adsorption process. These results demonstrate that the as-prepared FC515 owns the superior Cr(VI) adsorption performance.

Figure 3b displays the q_t of Cr(VI) on FC515 at temperature of 298, 308, and 318 K. It's observed that the Cr(VI) adsorption on FC515 is significantly decreased with increasing temperature from 298 to 318 K and the maximum Cr(VI) q_t on FC515 is determined to be 9.523, 8.667 and 7.672 mg·g^{-1} from Langmuir model for temperature of 298, 308, and 318 K, respectively. This indicates that the Cr(VI) adsorption process on FC515 is an exothermic process. The thermodynamic parameters including standard Gibb's free energy change (ΔG^0, kJ mol^{-1}), standard enthalpy change (ΔH^0, KJ mol^{-1}) and standard entropy change in entropy (ΔS^0, J mol^{-1} K^{-1}) are calculated in accordance with Equation (S9) and (S10) as well as Figure S5[30] and listed in Table S4. It's found that the ΔG^0 is negative at the measured temperature range, suggesting that the adsorption process of Cr(VI) on FC515 is thermodynamically feasible and spontaneous.[31] Meanwhile, it's also observed that the ΔG^0 values for the different temperatures are close to each other (-38.97, -40.11, and -41.29 kJ mol^{-1} for 298, 308, and 319 K, respectively). Meanwhile, it's shown that the ΔH^0 is negative, which means that the Cr(VI) adsorption on FC515 is an exothermic and energetically stable process.[32] This is accordant with the result obtained at the beginning of this part displaying that the adsorption of Cr(VI) onto FC515 is decreased with increasing temperature. It's reported that the absolute value of ΔH^0 ranges for physisorption and chemisorption are 2.1-20.9 and 80-200 KJ mol^{-1}, respectively.[33] In this work, the value of ΔH^0 is -4.397 KJ mol^{-1}, which also implies that the Cr(VI) adsorption on FC515 is mainly physisorption in nature. The positive ΔS^0 (115.996 J mol^{-1} K^{-1}) depicts the increased degree of freedom at the solid-liquid interface[34] during the adsorption of Cr(VI) on FC515.

The Cr(VI) adsorption behavior is strongly dependent on the solution pH.[35] The pH effect on Cr(VI) adsorption by FC515 is illustrated in Figure 4a. Noticeably, the Cr(VI) removal percentage is in-

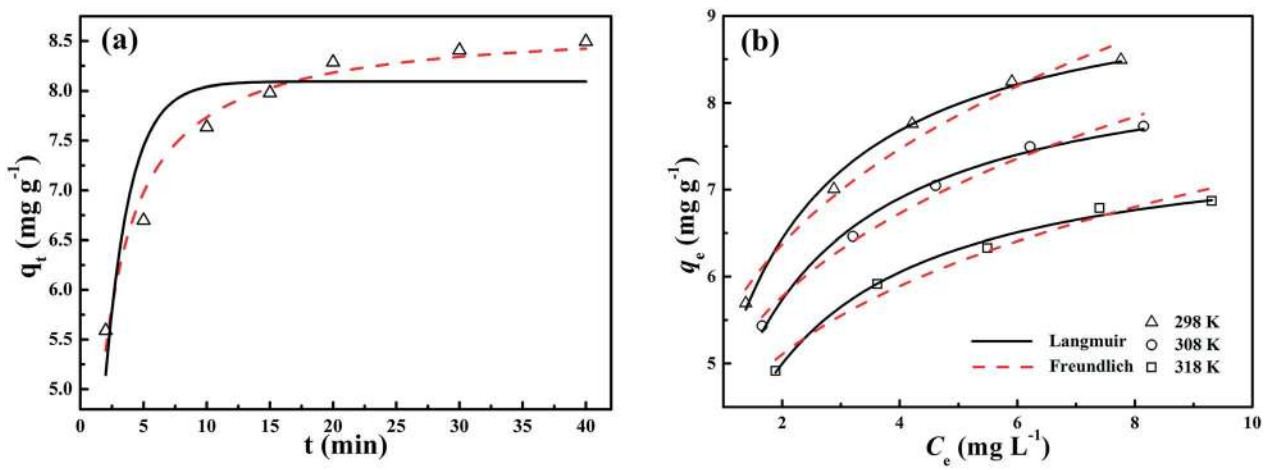

Fig. 3 (a) Effect of treatment time on Cr(VI) adsorption by FC515 (FC515 = 0.5 g L^{-1}, Cr(VI) = 6.5 mg L^{-1}, T = 298 K, pH = 3.0. The solid lines are the pseudo-first-order model; the dashed lines are the pseudo-second-order model); (b) Cr(VI) adsorption isotherm on FC515 (FC515 = 0.5 g L^{-1}, pH = 3.0) at 298, 308, and 318 K.

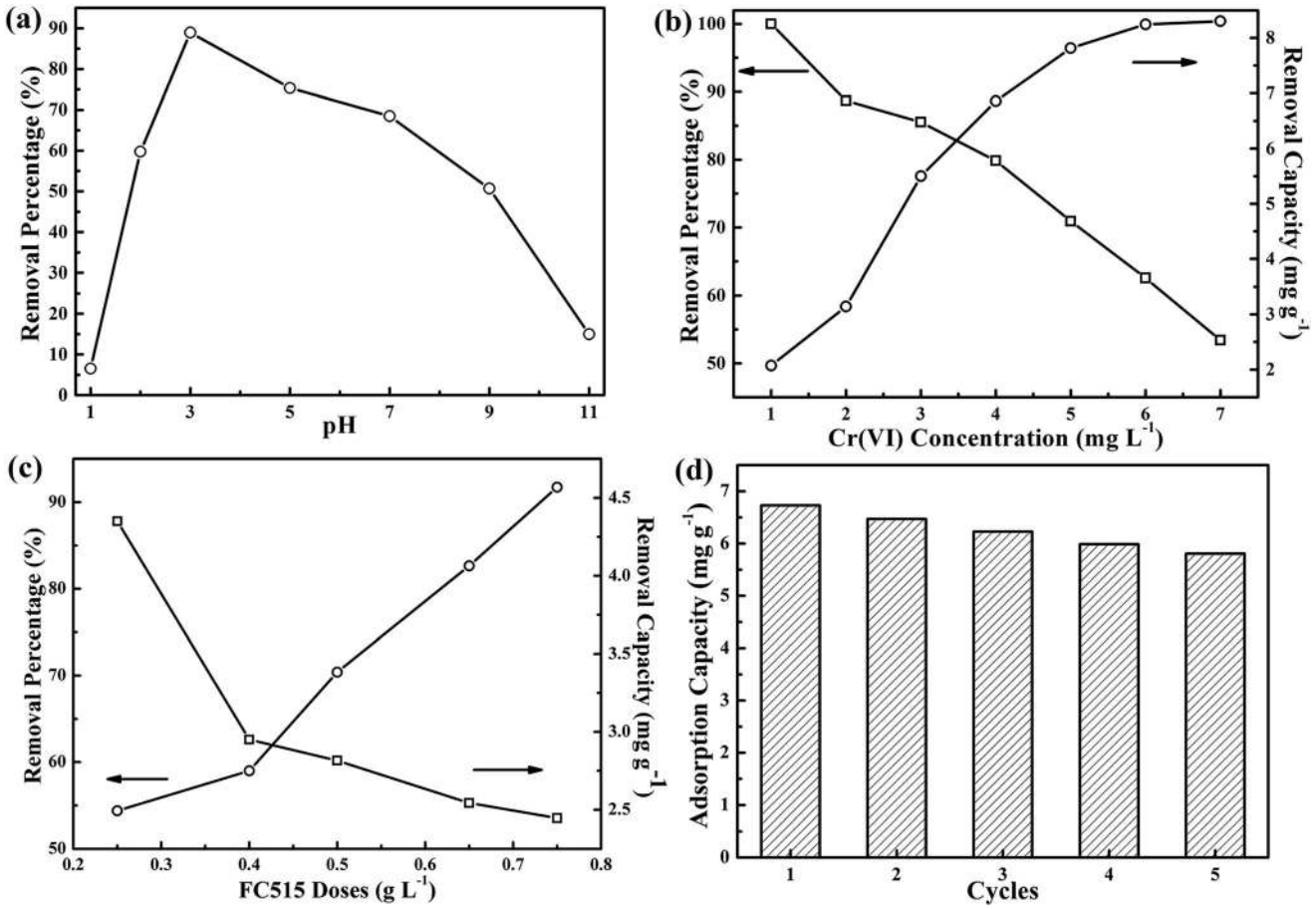

Fig. 4 Effect of (a) pH on Cr(VI) adsorption by FC515 (FC515 = 0.5 g L^{-1}, Cr(VI) = 2.0 mg L^{-1}, T = 298 K); and (b) initial Cr(VI) concentration on Cr(VI) adsorption by FC515 (FC515 = 0.5 g L^{-1}, pH = 3.0, T = 298 K); (c) FC515 dosages on Cr(VI) adsorption by FC515 (Cr(VI) = 5.0 mg L^{-1}, pH = 3.0, T = 298 K); (d) Cr(VI) adsorption capacity retention on FC515 (FC515 = 0.5 g L^{-1}, Cr(VI) = 15.5 mg L^{-1}, T = 298 K, pH = 3.0).

creased with increasing solution pH from 1.0 to 3.0, and then decreased with further increasing solution pH to 11.0. The Cr(VI) removal percentage on FC515 in the solution pH of 3.0 reaches the maximum value of 89.1%. The Cr(VI) removal percentage of FC515 in the solution pH values of 5.0, 7.0, 9.0, and 11.0 is 75.4%, 68.5%, 50.7% and 15.0%, respectively. Therefore, the solution pH 3.0 is the best value for FC515 to remove Cr(VI) from polluted water.

In the effect of initial Cr(VI) concentrations on Cr(VI) removal from polluted water, Figure 4b, 10.0 mg of FC515 is able to complete remove a 1.0 mg L^{-1} of Cr(VI) within a treatment period of 5 min. As the initial Cr(VI) concentration varies from 1.0 to 7.0 mg L^{-1}, the Cr(VI) removal percentage is gradually decreased. The removal percentage for the initial Cr(VI) concentration of 7.0 mg L^{-1} is reduced to 53.4%. In contrast, when the initial Cr(VI) concentration changes from 1.0 to 7.0 mg L^{-1}, the q_t of Cr(VI) on FC515 increases from 2.1 to 8.3 mg L^{-1}. In the solution with low Cr(VI) concentration (1.0-5.0 mg L^{-1}), the q_t increases rapidly, then increases slowly and gradually becomes stable in the solution with high Cr(VI) concentration (5.0-7.0 mg L^{-1}). This phenomenon may be due to the fact that FC515 has a limited amount of Cr(VI) adsorption active sites. In solution with the high Cr(VI) concentration, more Cr(VI) ions gradually occupy the active sites, causing the saturation of FC515 active site, so that the q_t is increased slowly.

In practice, the amount of adsorbent is an important factor affecting the adsorption performance.[14] The effect of FC515 dosages on the Cr(VI) removal in the solution with initial Cr(VI) concentration of 5.0 mg L^{-1} is described in Figure 4c. It's observed that the Cr(VI) removal percentage increases with the increase of FC515 dosages. As the FC515 dosage is changed from 0.25 to 0.75 g L^{-1}, the Cr(VI) removal percentage is increased from 54.4 to 91.8%. However, the q_t on FC515 tends to decrease with the increasing FC515 amounts. When the dosage of FC515 differs from 0.25 to 0.75 g L^{-1}, the Cr(VI) q_t on FC515 is declined from 4.4 to 2.5 mg g^{-1}. Since the Cr(VI) concentration in the aqueous solution is constant, with the increase of FC515 dosage, the number of active sites in the unsaturated sites is increasing, which leads to the decrease of q_t.

Figure S6 shows the Cr(VI) removal percentage by Fe_3O_4, carbonized chitosan coated Fe_3O_4 and FC515. It's believed that the as-synthesized FC 515 reveals the best Cr(VI) adsorption performance among these three materials (The Cr(VI) removal percentage for Fe_3O_4, carbonized chitosan coated Fe_3O_4 and FC515 is 32.1, 70.5, and 89.1%, separately.), verifying the role in the presence of carbonized *g*-PS.

In order to evaluate the possibility of regeneration and reuse of FC515 for practical application, the adsorption-desorption experiments were performed. The adsorption-desorption process was conducted for 5 cycles and the obtained q_t on FC515 is demonstrated in Figure 4d. It's found that the q_t on FC515 still remains around 86% after 5th cycles, illustrating a relatively good reusability and stability. This indicates that the FC515 is a good and reversible efficient nanoadsorbent in potential practical application for wastewater treatment.

3.4. Adsorption mechanism exploration of FC515 in optimal adsorption condition

In the aqueous solution, the most important forms of Cr(VI) are CrO_4^{2-}, $Cr_2O_7^{2-}$, $HCrO_4^-$ and H_2CrO_4, the presence of these ions is closely related to the pH of solution. As the pH is less than 6.8, the $HCrO_4^-$ is the predominant form. And CrO_4^{2-} and $Cr_2O_7^{2-}$ are the most stable forms present when the pH is above 6.8. However, the isoelectric point of FC515 is at a pH of about 4.7, as shown in Figure 5a, the surface of the FC515 is positively charged at a pH of 3.0. According to the principle of electrostatic interaction, there is an electrostatic attraction between FC515 and Cr(VI). Therefore, at the optimum pH of 3.0, the removal of Cr(VI) is mainly caused by electrostatic attraction.

In order to further study the removal mechanism of Cr(VI) on FC515, XPS analysis of FC515 after adsorption was carried out. High resolution XPS is applied to determine the chemical state of Cr element. Generally, in the high resolution XPS curve of Cr2p, the characteristic binding peak position appears at 577.0-578.0 eV and 586.0-588.0 eV, attributing to Cr(III).[36] The characteristic binding energy peak position typically occurred at 580.0-580.5 and 589.0-590.0 eV is usually ascribed to Cr(VI).[2] Figure 5b shows the Cr2p high resolution XPS peak spectrum of 20.0 mL Cr(VI) solution with the concentration of 10.0 mg L^{-1} and pH 3.0 after treatment with FC515 for 5 min. Evidently, the characteristic binding energy peak position of Cr2p is located at 580.1 and 589.4 eV, respectively, which are the characteristic binding energy peak of Cr(VI). This indicates that the absorbed species on the surface of the FC515 are Cr (VI). In summary, the results show that the Cr(VI) removal

Fig. 6 Proposed adsorption mechanism of Cr(VI) by FC515 in optimal adsorption condition.

on FC515 is a simple electrostatic adsorption process accompanying with physisorption as determined from thermodynamic analysis. The proposed Cr(VI) adsorption on FC515 is illustrated in Figure 6.

4. Conclusion

In this work, the Cr(VI) adsorption performance by chitosan-coated-magnetite with covalently *g*-PS based magnetic carbon nanocomposites has been evaluated. The magnetic carbon nanocomposite FC515 calcined at a temperature of 500 °C for 15 min in the N_2 atmosphere exhibits the highest Cr(VI) removal ability. The SEM and TEM images indicate that the FC515 consists of carbon-coated Fe_3O_4 nanoparticles embedded on the surface of carbonized PS microsphere. The optimum pH for Cr(VI) removal on FC515 is 3.0 at 298 K. The Cr(VI) removal percentage decreases with increasing the initial concentration of Cr(VI) and increases with the increase of FC515. The Cr(VI) adsorption behavior on FC515 obeys the pseudo-second order kinetic equation and the Langmuir isothermal adsorption model, indicating that the Cr(VI) adsorption on FC515 is monolayer adsorption. The thermodynamic analysis

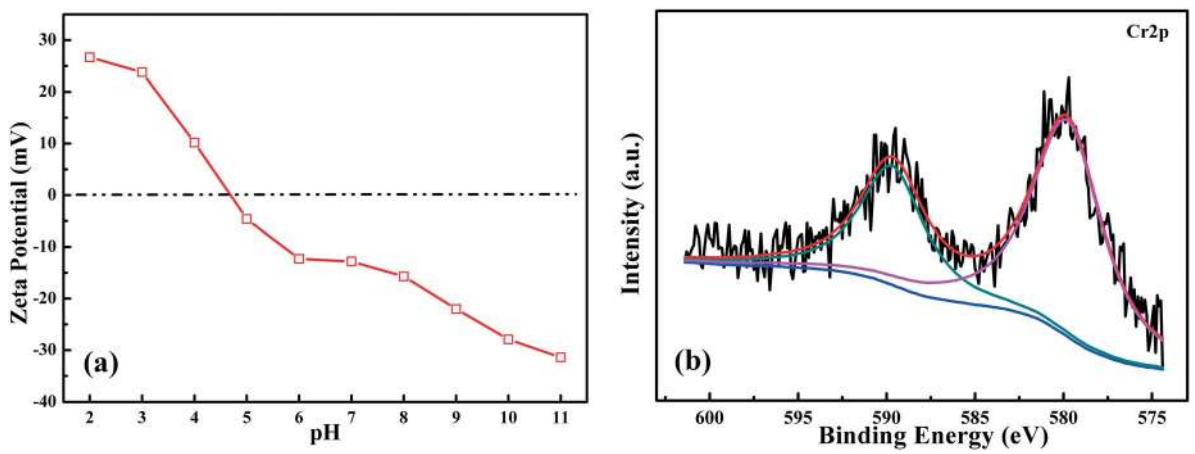

Fig. 5 (a) Zeta potential as a function of pH for FC515; (b) high resolution XPS of adsorbed Cr on FC515.

proves that Cr(VI) adsorption process on FC515 is a spontaneous exothermic process and reduce the temperature could boost the adsorption process. After the recovery and reuse by the permanent magnet after 5 times, FC515 still maintains more than 86% of adsorption performance, expressing a good stability and reusable capability. The zeta potential and XPS results illustrate that the Cr (VI) removal by FC515 in the solution of pH 3.0 is mainly related to the electrostatic interaction.

Supporting Information

Additional Experimental parts, Table S1-S4, and additional Figures S1-S6 are provided.

Funding information

The authors are grateful for the support and funding from the Foundation of National Natural Science Foundation of China (No. 51703165), Shanghai Science and Technology Commission (14DZ2261100), Young Elite Scientist Sponsorship Program by CAST (YESS, No. 2016QNRC001). The work is supported by special fund of State Key Joint Laboratory of Environment Simulation and Pollution Control (17K02ESPCT).

References

1 X. Xu, H. Zhang, C. Ma, H. Gu, H. Lou, S. Lyu, C. Liang, J. Kong and J. Gu, *J. Hazard. Mater.*, 2018, **353**, 166–172.
2 H. Gu, H. Lou, D. Ling, B. Xiang and Z. Guo, *RSC Adv.*, 2016, 110134–110145.
3 W. Yin, Y. Li and J. Wu, et al., *J. Hazard. Mater.*, 2017, **332**, 42–50.
4 P. V. Krivoshapkin, I. V. Mishakov, A. A. Vedyagin, Y. I. Bauman and E. F. Krivoshapkina, *Compos. Commun.*, 2017, **6**, 17–19.
5 S.-P. Kuang, Z.-Z. Wang, J. Liu and Z.-C. Wu, *J. Hazard. Mater.*, 2013, **260**, 210–219.
6 L. Zhou, J. Xu, X. Liang and Z. Liu, *J. Hazard. Mater.*, 2010, **182**, 518–524.
7 G. Dodi, D. Hritcu, G. Lisa and M. I. Popa, *Chem. Eng. J.*, 2012, **203**, 130–141.
8 W. S. Wan Ngah, L. C. Teong and M. A. K. M. Hanafiah, *Carbohydr. Polym.*, 2011, **83**, 1446–1456.
9 R. Laus, T. G. Costa, B. Szpoganicz and V. T. Fávere, *J. Hazard. Mater.*, 2010, **183**, 233–241.
10 M.-T. Wu, Y.-L. Tsai, C.-W. Chiu and C.-C. Cheng, *RSC Adv.*, 2016, **6**, 104754–104762.
11 Y. Chen and J. Wang, *Chem. Eng. J.*, 2011, **168**, 286–292.
12 Y. Zhu, J. Hu and J. Wang, *J. Hazard. Mater.*, 2012, **221**, 155–161.
13 L. Zhou, J. Jin, Z. Liu, X. Liang and C. Shang, *J. Hazard. Mater.*, 2011, **185**, 1045–1052.
14 H. Gu, H. Lou, J. Tian, S. Liu and Y. Tang, *J. Mater. Chem. A*, 2016, **4**, 10174–10185.
15 G. Yu, Y. Lu and J. Guo, et al., *Adv. Comp. Hybrid Mater.*, 2018, **1**, 56–78.
16 H. Gu, C. Ma, C. Liang, X. Meng, J. Gu and Z. Guo, *J. Mater. Chem. C*, 2017, **5**, 4275–4285.
17 H. Gu, H. Zhang and C. Ma, et al., *J. Phys. Chem. C.*, 2017, **121**, 13265–13273.
18 M. M. Ghobashy and M. A. Elhady, *Compos. Commun.*, 2017, **3**, 18–22.
19 H. Wu, Y. Zhang, R. Yin, W. Zhao, X. Li and L. Qian, *Adv. Comp. Hybrid Mater.*, 2018, **1**, 168–176.
20 H. Wei, H. Gu and J. Guo, et al., *Adv. Comp. Hybrid Mater.*, 2018, **1**, 127–134.
21 L.F. Velasco, R. Guillet-Nicolas, G. Dobos, M. Thommes and P. Lodewyckx, *Carbon*, 2016, **96**, 753–758.
22 B. Xiang, D. Ling, H. Lou and H. Gu, *J. Hazard. Mater.*, 2017, **325**, 178–188.
23 H. Gu, S. Tadakamalla and Y. Huang, et al., *ACS Appl. Mater. Interfaces.*, 2012, **4**, 5613–5624.
24 T.A. Saleh, *Water Treat.*, 2015, **57**, 10730–10744.
25 J. Zhu, S. Wei and H. Gu, et al., *Environ. Sci. Technol.*, 2012, **46**, 977–985.
26 J. Zhu, H. Gu and S. B. Rapole, et al., *RSC Adv.*, 2012, **2**, 4844–4856.
27 Q. Li, L. Sun, Y. Zhang, Y. Qian and J. Zhai, *Desalination*, 2011, **266**, 188–194.
28 Y. Zhang, Y. Tang, S. Li and S. Yu, *Chem. Eng. J.*, 2013, **222**, 94–100.
29 K. Z. Setshedi, M. Bhaumik, M. S. Onyango and A. Maity, *Chem. Eng. J.*, 2015, **262**, 921–931.
30 J. Fu, Z. Chen and M. Wang, et al., *Chem. Eng. J.*, 2015, **259**, 53–61.
31 Y. Wu, H. Luo, H. Wang, C. Wang, J. Zhang and Z. Zhang, *J. Colloid Interface Sci.*, 2013, **394**, 183–191.
32 L. Liu, Y. Lin, Y. Liu, H. Zhu and Q. He, *J. Chem. Eng. Data.*, 2013, **58**, 2248–2253.
33 H. Li, F. Zaviska, S. Liang, J. Li, L. He and H.Y. Yang, *J. Mater. Chem. A*, 2014, **2**, 3484–3491.
34 G. Zhao, J. Li and X. Wang, *Chem. Eng. J.*, 2011, **173**, 185–190.
35 G. Zhu, J. Liu and J. Yin, et al., *Chem. Eng. J.*, 2016, **288**, 390–398.
36 H. Wang, X. Yuan and Y. Wu, et al., *Chem. Eng. J.*, 2015, **262**, 597–606.

